1000-0569/2007/023(01)-0083-92 *Acta Petrologica Sinica* 岩石学报

Generation and evolution of Cenozoic alkaline rocks from the Chukchi peninsula, Russia: Insight from melt and fluid inclusions

Irina P. Solovova[1], Theodoros Ntaflos[2], Andrei Girnis[1*], Natalya N. Kononkova[3] and Vyacheslav V. Akinin[4]

1. *Institute of Geology of Ore Deposits, Petrography, Mineralogy, and Geochemistry*, 35 *Staromonetny*, *Moscow*, 119017, *Russia*
2. *Institute of Mineralogy*, *University of Vienna*, *Austria*
3. *Vernadsky Institute of Geochemistry and Analytical Chemistry*, *Moscow*, *Russia*
4. *Northeastern Interdisciplinary Research Institute*, *Magadan*, *Russia*

Received: 2006-07-12 *Accepted*: 2006-11-20

Solovova I P, Ntaflos T, Girnis A, Kononkova N N and Akinin V V. 2007. Generation and evolution of Cenozoic alkaline rocks from the Chukchi peninsula, Russia: Insight from melt and fluid inclusions. ***Acta Petrologica Sinica*****, 23(1):83-92**

Abstract Melt and fluid inclusions were studied in the minerals of Cenozoic olivine melanephelinites from the Chukchi Peninsula, Russia. The rock contain several generations of olivine phenocrysts varying in composition at mg = 0.88 ~ 0.77. The phenocrysts bear fluid and melt inclusions recording various stages of melt crystallization in volcanic conduits and shallow magma chambers. Primary fluid inclusions are CO_2-dominated with a density of up to 0.93 g/cm^3. All fluid inclusions are partially leaked, which is indicated by haloes of tiny fluid bubbles around large fluid inclusions in minerals. Melt inclusions contain various daughter crystals, which were completely resorbed in thermometric experiments at about 1230℃. Assuming that this temperature corresponds to the entrapment conditions of the CO_2 fluid inclusions, the minimum pressure of the beginning of magma degassing is estimated as 800MPa. Variations in the compositions of homogenized silicate melt inclusions indicate that olivine was the earliest crystalline phase followed by clinopyroxene, nepheline and orthoclase. This sequence is in agreement with the mineralogy of the rocks. The melts are strongly enriched in incompatible trace elements and volatiles (in addition to CO_2, high Cl, F, and S contents were detected). There are some differences between the compositions of melts trapped in minerals from different samples. Variations in SiO_2, FeO, and incompatible element contents are probably related to melt generations at various levels in a homogeneous mantle reservoir.

Key words Chukchi Peninsula, Melanephelinite, Inclusion, Melt, Fluid

1 Introduction

The Bering Sea basaltic province includes several Late Cenozoic volcanic occurrences in Alaska, Chukchi Peninsula, and Bering Sea islands (Moll-Stalcup, 1994). In contrast to the Aleutian island arc, the petrology and geochemistry of these occurrences have been studied only fragmentarily (e. g. Kay *et al.*, 1978; Feeley and Winer, 1999). Alkaline rocks from the eastern part of this region, the southern coast of the Chukchi Peninsula, Russia, were recently described by Akinin (1994), Akinin and Apt (1994), Apt *et al.* (1998) (Fig. 1). The magmatic activity of the Chukchi Peninsula is related to intraplate continental rifting (Fedorov and Seregina, 1990; Fedorov *et al.*, 1993). The Sr, Nd, and Pb isotopic compositions of igneous rocks and xenoliths from this complex suggested that the most primitive alkaline magmas could be derived from a slightly depleted mantle peridotite that had been enriched by incompatible trace elements shortly before the eruption (Apt *et al.*, 1998).

These volcanics make up lava flows, plugs, domes, and scoria cones (Akinin, 1994). Their K-Ar age is ca. 6 Ma (Akinin and Apt, 1994). The most common rocks are olivine melanephelinites. In addition, there are leucite-bearing olivine tephrites and other alkaline rocks. Akinin (1994) and Akinin *et al.* (1997) studied mantle nodules from these rocks and argued that the primary melanephelinite magma was generated at pressures of 3.0 ~ 3.2GPa (depth of about 100km) and temperatures of 1300 ~ 1320℃. In this paper we present the results of an investigation of melt and fluid inclusions in the minerals of the olivine melanephelinites, which provided new insight into the conditions of magma generation, crystallization, and degassing.

* E-mail: girnis@igem.ru

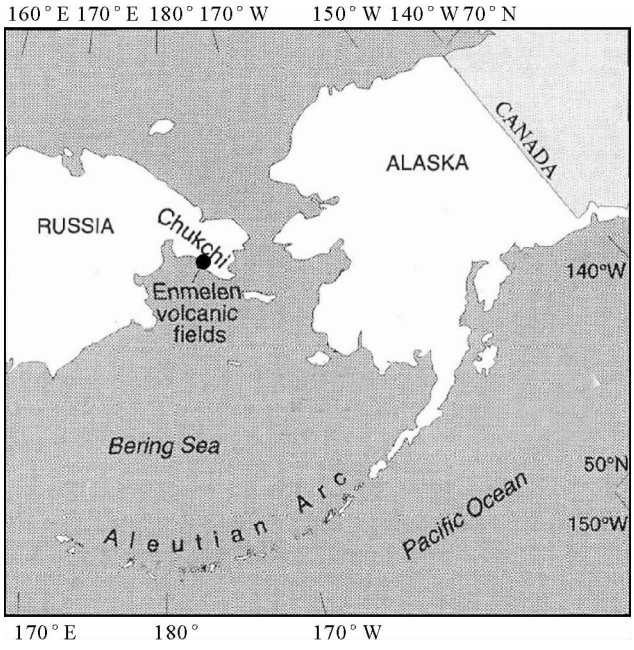

Fig. 1 Location of the Chukchi Peninsula and Enmelen Volcanic Fields in the Bering Sea region (after Akinin *et al.*, 2005).

2 Methods

Inclusions were studied in double-polished sections, 0.3 mm thick. Heating experiments were conducted in electric furnaces with Pt-Rh heaters (up to 1500℃) using graphite containers to prevent mineral oxidation. Temperature was measured by a Pt-Rh thermocouple calibrated against the melting point of gold (1063℃). The rate of heating varied from 2 to 80℃/min, and samples were kept at a desired temperature for 10 to 60 min (usually, 15 min). Fluid inclusions were explored on a Linkam-THMSG 600 cryogenic stage cooled with liquid nitrogen and calibrated using synthetic fluid inclusions of CO_2 or aqueous NaCl solutions of known concentrations. The rate of heating and cooling varied from 0.5 ~ 50℃/min, and exposure was up to 5min. Some phases were identified by Raman spectroscopy by E. Libowitzki (Institute of Mineralogy, University of Vienna, Austria).

Minerals and glasses were analyzed with a Cameca MS-46 electron microprobe at the Vernadsky Institute of Geochemistry and Analytical Chemistry, Russian Academy of Sciences and a Cameca SX-100 electron microprobe at the Institute of Mineralogy, University of Vienna. Minerals were analyzed by a focused beam, and glasses were scanned over areas of 5 × 5 or 12 × 12μm to minimize Na loss. Natural minerals and glasses were used as standards.

Trace and volatile elements were analyzed with a Cameca IMS-4f ion microprobe at the Institute of Microelectronics, Russian Academy of Sciences (Yaroslavl, Russia, analyst S. Simakin). A beam of primary O_2^- ions accelerated to 10keV was focused on the sample surface to a 20μm diameter spot using a field aperture. The beam current was 3 ~ 6nA. Sputtered secondary ions were analyzed in five accumulation cycles.

3 Petrography and mineralogy

Seven melanephelinite samples from lava flows were studied. They are massive (samples N-2, N-6 and N-7) or porous (samples N-4, N-3, Gyd-2, and Teph-1) dark gray porphyritic rocks. All the samples show similar mineralogical characteristics.

The groundmass (Tables 1 ~ 4) consists of olivine ($mg = Mg/(Mg + Fe^{2+}) = 0.76 \sim 0.78$), clinopyroxene ($mg = 0.74 \sim 0.59$), plagioclase, anorthoclase, alkali feldspar varying from albite to orthoclase, nepheline, F-apatite, Ti-magnetite, and ilmenite (in sample Teph-1).

Olivine grains, up to 600μm in size, are predominant among phenocrysts. The crystals are fresh and sometimes show distinct faces or skeletal shapes with deep embayments of crystallized groundmass. Partially resorbed olivine grains are common in samples N-2 and N-3. Their composition ($mg = 0.83 \sim 0.86$ and 0.3 ~ 0.4wt% CaO) suggests that they could be the earliest phenocrysts.

The composition of olivine from samples N-2, N-3, N-4, N-7, and Teph-1 varies within $mg = 0.86 \sim 0.77$ and 0.3 ~ 0.5wt% CaO (Table 4). The olivine of sample Gyd-2 is slightly more magnesian, $mg = 0.85 \sim 0.88$, but its CaO content is similar, 0.26 ~ 0.41wt% (Fig. 2). Even in small phenocrysts, the compositions of central and rim zones may be significantly different, for instance, $mg = 0.81$ and $mg = 0.74$, respectively (Table 4, an. 19 and 20). The concentrations of CaO and MnO are in general negatively correlated with mg values (Fig. 2).

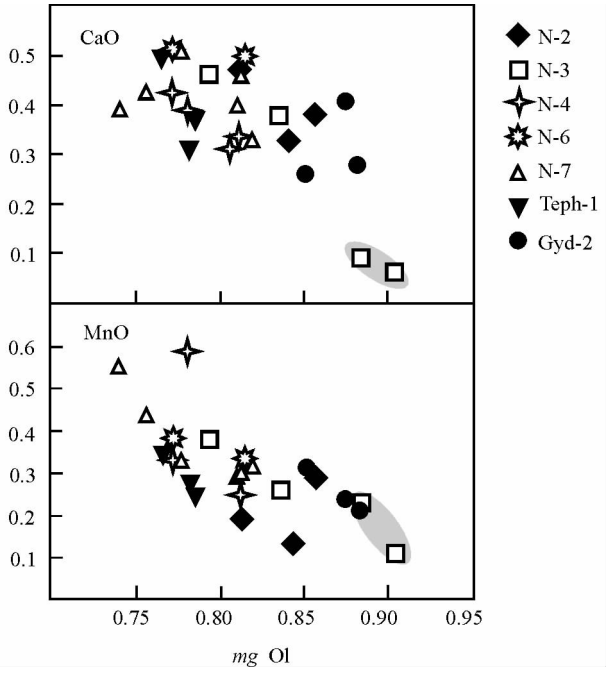

Fig. 2 Correlation of CaO and MnO concentrations in olivine with mg = Mg/(Mg + Fe). The shaded field shows olivine xenocrysts.

Table 1 Microprobe analyses of groundmass phases, wt%

	Phase	SiO_2	TiO_2	Al_2O_3	FeO	MgO	CaO	Na_2O	K_2O	BaO	SrO	Total	*mg*
1	Ol	39.00	0.07	0.13	22.19	40.16	0.50	0.00	0.00	0.06	0.00	102.11	0.76
2	Ol	38.11	0.06	0.00	20.25	40.12	0.31	0.00	0.00	0.00	0.00	98.85	0.78
3	Ol	38.96	0.08	0.00	21.43	39.52	0.48	0.00	0.00	0.10	0.00	100.57	0.77
4	Cpx	50.90	4.29	8.49	7.00	5.74	22.72	0.61	0.00	0.11	0.00	99.86	0.59
5	Cpx	50.51	3.27	4.74	7.18	10.73	22.14	0.92	0.31	0.10	0.00	99.90	0.73
6	Cpx	50.29	3.05	5.33	6.42	10.11	22.79	0.59	0.00	0.12	0.09	98.79	0.74
7	Pl	57.11	0.22	25.32	0.32	0.10	9.38	5.98	0.57	0.30	0.90	100.20	—
8	Fsp	56.23	0.20	29.18	1.11	0.40	0.26	11.23	1.39	0.00	0.00	100.00	—
9	Fsp	62.41	0.22	21.78	1.01	0.37	2.01	6.95	4.76	0.00	0.11	99.62	—
10	Ab	60.81	0.00	26.47	1.43	0.67	0.00	9.23	0.34	0.10	0.00	99.05	—
11	Or	59.81	0.17	21.84	0.30	0.09	0.00	0.12	18.14	0.06	0.00	100.53	—
12	Or	59.80	0.14	21.98	1.29	0.36	0.07	0.12	16.29	0.01	0.00	100.06	—
13	Ol	37.92	0.00	0.15	19.94	39.99	0.46	0.00	0.00	0.06	0.13	98.65	0.78
14	Cpx	47.61	3.43	5.39	7.34	13.36	23.29	0.69	0.00	0.00	0.10	101.21	0.76
15	Ne	45.65	0.13	31.39	1.60	0.66	1.05	14.60	4.72	0.00	0.16	99.96	—
16	Ne	45.98	0.09	32.29	1.73	0.83	0.41	15.06	4.91	0.00	0.00	101.30	—
17	Cpx	52.49	1.72	1.31	6.35	14.61	22.83	1.03	0.00	—	—	100.34	0.80
18	Ne	44.10	0.13	33.85	1.54	0.10	0.35	16.38	4.64	—	—	101.09	—

reviations: Ab, albite; Cpx, clinopyroxene; Fsp, feldspar; Ne, nepheline; Ol, olivine; Or, ortoclase; Pl, plagioclase.

Table 2 Analyses of opaque minerals, wt%

	Ti-Mt	Ilm	Sp	Sp	Sp	Sp	Ilm
	1	2	3	4	5	6	7
FeO	70.64	40.07	64.98	36.63	38.34	62.37	40.67
TiO_2	21.85	50.39	11.65	17.85	3.38	14.02	50.15
MnO	0.62	0.54	0.57	0.25	0.29	0.34	0.94
MgO	4.14	5.95	5.88	9.73	9.61	6.95	5.58
Al_2O_3	2.10	0.49	7.02	10.44	21.18	5.89	0.04
SiO_2	0.29	1.07	0.69	1.07	1.00	0.03	0.50
CaO	0.08	0.22	0.08	0.25	0.08	0.02	0.09
Cr_2O_3	—	—	7.57	23.72	24.66	4.85	0.05
Total	99.72	98.73	98.44	99.94	98.54	94.47	98.02

Note: (1 ~ 2) Sample Teph-1, groundmass; (3 ~ 6) crystalline inclusions in olivine from sample (3) N-4, (4 ~ 5) Gyd-2, and (6) N-7. (7) Small grain from glass in Lc-bearing xenolith.

Table 3 Analyses of apatite from rock groundmass, wt%

	CaO	P_2O_5	FeO	BaO	SrO	SiO_2	F	Total
1	55.80	40.34	0.84	0.03	0.41	0.77	3.57	101.76
2	53.99	39.89	0.42	0.00	0.43	1.08	3.47	99.28
3	54.05	38.39	0.56	0.14	0.33	1.92	3.35	98.74
4	52.52	39.22	0.37	0.17	0.27	0.76	3.55	96.86
5	51.87	37.53	0.28	0.00	0.29	0.91	3.89	94.77
6*	56.00	—	—	0.12	2.90	1.50	—	

Note: (1 ~ 5) Sample Teph-1 and (6) Sample N-4. * Semiquantitative analysis of apatite grain in a fracture in olivine; 0.2 wt% Cl.

Table 4 Representative microprobe analyses of olivine, wt%

	Sample	SiO_2	MgO	FeO	MnO	CaO	Total	*mg*
1	N-2	35.30	44.33	18.30	0.19	0.47	98.59	0.81
2		36.59	47.20	15.70	0.14	0.33	99.96	0.84
3	N-3	40.50	50.27	9.51	0.11	0.06	100.45	0.90
4		40.37	48.99	11.42	0.23	0.09	101.10	0.88
5		38.93	44.01	15.42	0.26	0.38	99.00	0.78
6		36.82	41.32	19.11	0.38	0.46	98.09	0.84
7	N-4	38.82	41.29	17.36	0.25	0.34	98.06	0.80
8		39.31	39.45	21.19	0.33	0.43	100.71	0.81
9	N-6	40.53	41.73	16.91	0.34	0.50	100.00	0.81
10		38.77	38.81	20.39	0.38	0.51	98.86	0.77
11	N-7	36.69	44.95	17.69	0.32	0.33	99.98	0.82
12		35.95	41.33	21.21	0.33	0.51	99.33	0.78
13		39.62	42.37	17.97	0.29	0.4	100.65	0.81
14		38.41	37.94	23.72	0.55	0.39	101.01	0.74
15	Teph-1	39.12	40.11	19.82	0.25	0.37	99.67	0.79
16	Gyd-2	35.27	51.11	13.05	0.24	0.41	100.08	0.87
17		36.98	46.98	14.69	0.31	0.26	99.22	0.85

Note: Analyses nos. (3) and (4) are xenocrysts. Other analyses are various zones of phenocrysts. (13) and (14) are the center and rim of a single grain.

Table 5 Compositions of crystalline inclusions, daughter phases of melt inclusions, and minerals of a xenolith, wt%

	Phase	SiO_2	TiO_2	Al_2O_3	FeO	MnO	MgO	CaO	Na_2O	K_2O	BaO	Total	*mg*
1	Ne	43.30	0.00	30.51	1.93	0.05	0.57	0.00	14.50	7.83	0.02	98.71	—
2	Ne	43.25	0.08	32.14	1.49	0.00	0.37	0.08	15.45	6.09	0.05	99.00	—
3	Ne	42.74	0.09	31.61	1.52	0.08	0.40	0.08	15.73	5.92	0.04	98.21	—
4	Cpx	49.32	2.26	5.23	7.38	0.14	11.99	17.06	3.15	0.39	0.04	96.96	0.74
5	Cpx	48.88	3.29	4.30	6.95	0.09	13.48	22.20	1.67	0.30	0.09	101.38	0.78
6	Cpx	50.47	2.82	2.59	6.78	0.11	14.71	21.69	1.48	0.18	0.21	101.21	0.79
7	Cpx	49.59	2.46	2.41	6.62	0.14	14.39	21.79	1.30	0.34	0.11	99.15	0.79
8	Cpx	51.59	2.30	1.48	5.95	0.09	15.18	23.62	0.63	0.00	—	100.84	0.82
9	Ol	38.24	0.00	0.00	23.75	0.64	37.28	0.38	0.00	0.00	—	100.29	0.74
10	Ol	38.23	0.00	0.00	23.80	0.61	37.35	0.43	0.00	0.00	—	100.42	0.74
11	Cpx	54.55	0.14	0.41	6.55	0.20	16.98	20.34	1.06	0.04	—	100.27	0.82
12	Cpx	52.33	1.32	1.48	6.27	0.17	14.60	22.93	0.73	0.03	—	99.86	0.81
13	Cpx	54.54	0.10	0.27	6.67	0.16	16.12	21.16	1.16	0.17	—	100.35	0.81
14	Lc	56.55	0.09	24.72	1.24	0.00	0.09	0.07	0.47	17.72	—	100.95	—
15	Lc	55.79	0.12	24.52	1.01	0.00	0.00	0.04	0.50	17.43	—	99.41	—
16	Gl	61.40	1.08	15.72	5.46	0.10	1.18	1.43	4.42	5.47	—	96.26	0.28
17	Gl	57.30	1.40	17.37	4.44	0.08	2.97	1.22	5.87	5.85	—	96.50	0.54
18	Gl	61.93	0.29	21.56	3.23	0.06	0.72	0.07	3.72	4.84	—	96.42	0.28

Note: (1 ~ 4) Crystalline inclusions in olivine (1) Fo81.5 and (2) Fo77.2, (4) with 0.13wt% SrO and (6) with 0.17wt% SrO. (8) Clinopyroxene microphenocryst from sample N-7.
(9 ~ 18) Phases from a xenolith, sample N-7; (13) inclusion of clinopyroxene in olivine; (16 ~ 17) glassy melt inclusions in olivine; (18) glass between xenolith crystals.

Relatively large (up to 1mm) grains of fresh olivine with mg up to 0.90 and very low CaO (0.06wt% in the center and 0.09wt% near the rim) were found in sample N-3. Such grains in this and other samples were interpreted as xenocrysts. They are always free of primary inclusions.

Clinopyroxene phenocrysts are very rare. They form greenish yellow prisms up to a few hundreds of micrometers long. Since no inclusions were found in the clinopyroxene, it was not studied in detail. Nonetheless, several crystals were analyzed in sample N-7. They showed *mg* = 0.80 and contained about 1wt% Na_2O and 1.3wt% Al_2O_3 (Table 5, an. 8).

A xenolith, about 5 mm across, was found in sample N-7. It is composed of partly resorbed olivine and clinopyroxene grains cemented by glass. Olivine and clinopyroxene show *mg* values of 0.74 and 0.82, respectively, and contain rounded crystalline inclusions of leucite and primary melt inclusions consisting of glass and gas. The glass is very rich in alkalis (Table 5, an. 16 ~ 18) owing to olivine crystallization on the walls. This xenolith is probably a fragment of an earlier leucite-bearing rock, which is common in this region.

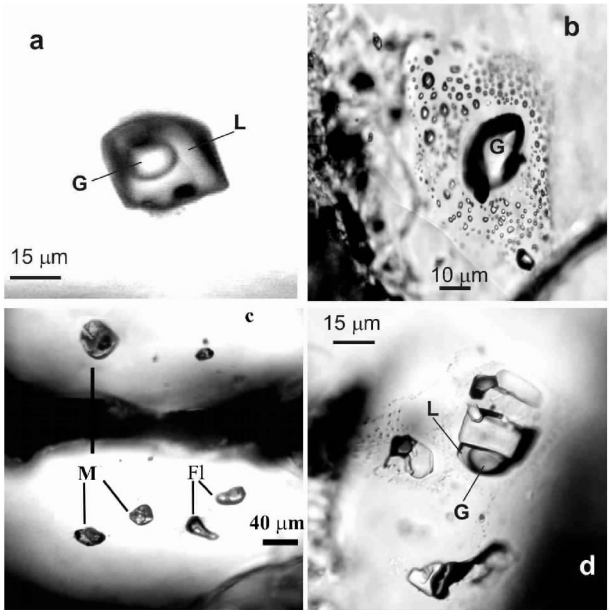

Fig. 3 Photomicrographs of fluid inclusions in olivine from sample N-4. (a) Primary two-phase inclusion with a tiny magnetite crystal on the wall. (b) Partially decrepitated secondary inclusion with gaseous CO_2. (c) Coexisting-melt and fluid inclusions in olivine. (d) Partially decrepitated primary melt inclusion with two-phase (liquid + gas) CO_2 fluid. L-liquid CO_2, G-gaseous CO_2, M-melt, and Fl - fluid.

4 Inclusions in minerals

The olivine phenocrysts contain melt, fluid, and monomineralic spinel inclusions. Inclusions of K-bearing nepheline and Ti-bearing clinopyroxene with 5wt% Al_2O_3 (Table 5) were found in olivine from sample N-6 .

4.1 Fluid inclusions

A remarkable feature of the alkaline volcanics is the abundance of CO_2 fluid inclusions (Fig. 3c). Primary and secondary fluid inclusions are composed of one (gas) or two (gas + liquid) phases and always bear evidence of partial leakage (Fig. 3a, 3b). Clusters of fluid and melt inclusions connected by narrow channels are very common in olivine. Fluid inclusions in such groups always consist of two phases and have a rather stable CO_2 density. In addition, some inclusions contain solid phases, among which magnetite was identified by Raman spectroscopy. Several 5-μm fluid inclusions consisting of liquid and several transparent crystals (without gas) were found in sample Gyd-2. The crystals were too small for Raman

investigations. The primary inclusions show inverse crystal shapes (Fig. 3a) and are no larger than 40μm, and the late and secondary inclusions are irregular in shape and may be as large as 100μm. Such inclusions are often connected with the rock groundmass. In such cases, large euhedral crystals form on the walls of inclusions. Grains with intense pleochroism from pink to dark brown (presumably, mica) were observed in the inclusions. The fluid phase has a low density, which is in accordance with the late-stage melt crystallization near the surface.

The material of fluid inclusions was frozen between −70 and −90℃, and thawed upon subsequent heating between −56.6. and −58.0℃. Only carbon dioxide was detected by Raman spectroscopy in an inclusion with a melting temperature of −56.7℃. The minimum homogenization temperature of CO_2 inclusions (1.9℃ in sample Gyd-2) corresponds to a fluid density of 0.93g/cm^3. The results of cryometric experiments are summarized in Table 6. At temperatures of 1200 ~ 1230℃, the CO_2 density variations (0.30 ~ 0.93 g/cm^3) correspond to pressures of 300 ~ 800MPa estimated from the PVT properties of pure CO_2 (Melnik, 1978; Shmonov *et al.*, 1974). The lowest CO_2 density was estimated from the volume of a low-density inclusion and the size of a CO_2 crystal that grew on its wall during cooling.

Several partially decrepitated melt inclusions (Fig. 3d) contained two-phase (liquid + gas) CO_2 fluid (Table 6). These inclusions are probably combined (melt + fluid). The density of CO_2 in them is 0.65 g/cm^3, corresponding to 300MPa at 1200℃.

Table 6 Results of fluid inclusion investigations

Sample	Type of inclusion	Tfr	Tm	Th	d, g/cm^3	T sil. melt	P, MPa
N-2	Primary, L + G	−87.3	−57.1	26.6	0.69	1200	370
	Primary, L + G	−81.2	−56.6	28.8	0.63	1200	320
	Secondary, L + G	−80.0	−57.4	23.8	0.74	1000	370
	Secondary, G	−71.1	−57.7	—	—	—	—
N-3	Primary, L + G	−69.3	−57.4	25.1	0.71	1100	370
	Primary, L + G	−79.3	−57.4	27.1	0.66		320
	Primary, G	−83.3	—	—	—	—	—
	Secondary, L + G	−71.5	−56.7	26.6	0.69	1100	360
	Secondary, G	−71.9	−56.7	—	—	—	—
N 4	Primary, L + G	−87.0	−57.2	22.4	0.75	1200	470
	Primary, L + G	−79.8	−56.9	29.0	0.65	1200	350
	Primary, G	−71.3	−57.0	—	0.24*	1200	70
	Primary, G	−70.0	−57.2	—	0.07*	—	—
	Secondary, G	−71.9	−56.7	—	—	—	—
	Fluid of melt incl., L + G	−84.5	−58.7	29.0	0.63	1150	300
	Fluid of melt incl., L + G		−58.3	28.0	0.66	1150	350
Gyd-2	Primary, L + G	−91.4	−57.7	−1.9	0.94	1200	800
	Secondary, L + G	−78.2	−56.9	23.2	0.74	1000	370
	Fluid of melt incl., G	−77.0	−56.6	—	—	—	—

Note: Temperatures in oC; Tfr-freezing; Th - homogenization; Tm - melting.
L - liquid and G - gas. All inclusions were partially decrepitated and produced liquid phase upon homogenization. T sil. melt is the homogenization temperature of coexisting silicate melt inclusions. P is pressure calculated for CO_2 density and T sil. melt.
* Fluid density calculated from the volume of CO_2 crystal grown within inclusions.

4.2 Melt inclusions

Melt inclusions in olivine (Fig. 4a) are usually no larger than 25 ~ 40μm (up to 70μm in sample Gyd-2). They are almost completely crystallized and contain olivine (on the walls), clinopyroxene, nepheline, and magnetite as daughter phases. Glass accounts for no more than a few percent by volume, and the shape of the gas phase is controlled by the surrounding crystals (Figs. 4b, 4c, 4d). Only olivine from sample Gyd-2 contains inclusions with large daughter crystals embedded in glass accounting for 20 30 vol % (Fig. 4c). The heterogeneity of the initial magma is supported by the occurrence of melt inclusions with up to 30 vol % of gas.

The beginning of melting was observed in the inclusions at 1100℃ (sample N-4), and daughter crystals were completely dissolved at 1210℃; thus, the melting interval is only 110℃. Complete homogenization was observed only in sample N-6 at 1200 ~ 1215℃. In all other cases, melt and gas were present in inclusions, and the volume of the gas vesicle was no more than 5 vol %. High-temperature experiments were halted when all daughter phases were resorbed (except for olivine on the walls of inclusions). Some vacuoles acquired inverse crystal outlines during heating (sample Gyd-2 at 1210℃, N-4 at 1230℃, and N-3 at 1180℃), which suggests that these experimental temperatures were close to the conditions of inclusion entrapment. Indirect evidence for high volatile contents in the

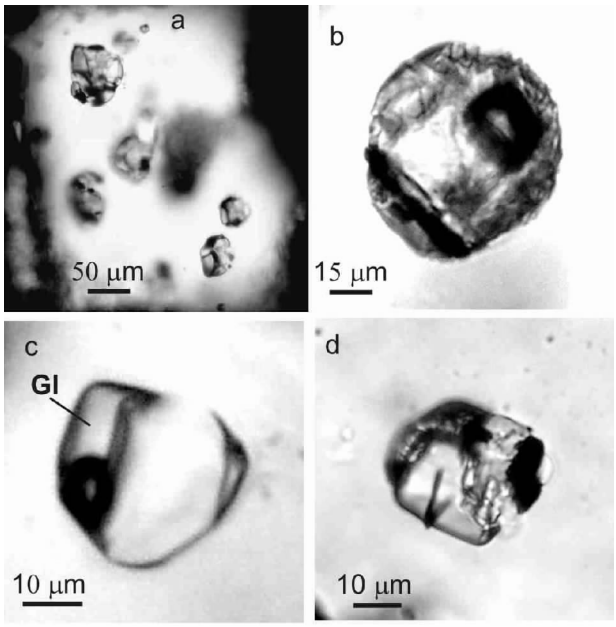

Fig. 4 Photomicrographs of primary melt inclusions in olivine. (a) Olivine crystal with melt inclusions, sample Teph-1. (b), (d) Fully crystallized melts with gas between crystals, samples N-6 and Teph-1, respectively. (c) Inclusion with about 30 vol % residual glass and a rounded gas bubble, sample N-4. Gl-glass.

system is provided by the presence of several gas bubbles in some inclusions heated above 1100℃ (sample N-4) or 1220℃ (Gyd-2). Partial leakage of inclusion material due to high internal gas pressure is common both in experiments and in nature (Fig. 3b).

4.3 Melt composition

Low-silica (37.5 ~ 40.5wt% SiO_2) alkaline magmas enriched in TiO_2 and P_2O_5 were trapped in melt inclusions. The concentration of CaO in the most magnesian (and iron-rich) melts is up to 11wt% . Melts from sample Gyd-2 are SiO_2 enriched compared with the other rocks but are strongly depleted in FeO and TiO_2 (Table 7, Fig. 5). The concentrations of other components are rather similar at a given MgO content.

The analysis of one sulfide-bearing inclusion (sample N-2) quenched from a temperature of 1200℃ showed 8.7wt% BaO and 1.2wt% SrO. The examination of this inclusion under high magnification (× 1000) revealed heterogeneity at a scale of about 0.5μm. The extremely high BaO and SrO concentrations are probably due to the entrapment of unknown Ba Sr-bearing phases coexisting with melt during olivine growth.

High concentrations of sulfur in the melts are in agreement with the occurrence of sulfide droplets in inclusions from samples N-2 and N-7. These inclusions show the maximum S concentrations (up to 0.27wt%).

Figure 5 illustrates variations in the chemistry of melt inclusions. The highest MgO (up to 10wt%) and FeO (up to 16wt%) concentrations were measured in olivine-hosted inclusions from samples N-2, N-3, and N-7. The melts contain about 7.5wt% of $K_2O + Na_2O$ with $Na_2O > K_2O$. The most

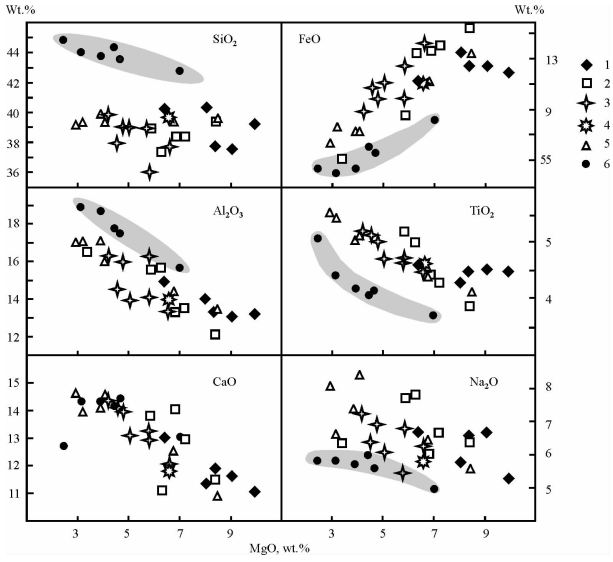

Fig. 5 Concentrations of major components in melts as functions of MgO. The fields of melt inclusions from sample Gyd-2 are shaded to emphasize the difference in melt composition. Symbols are the same as in Fig. 2.

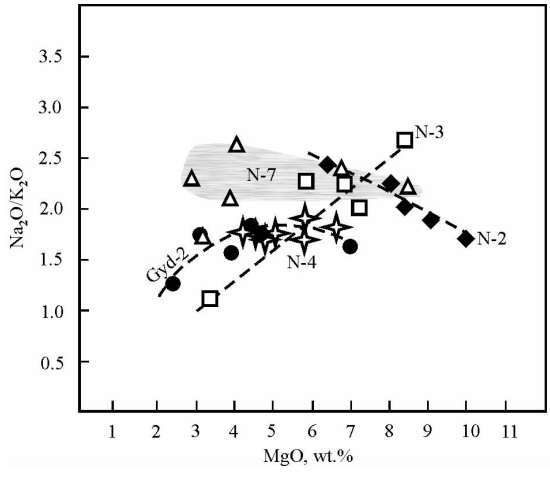

Fig. 6 Na_2O/K_2O value as a function of MgO concentration in homogenized melt inclusions in olivine. The shaded field corresponds to the compositions of melts from sample N-7. Symbols are the same as in Fig. 2.

evolved melts are enriched in Al, Ti, Ca, and Na. Their $K_2O + Na_2O$ values are up to 11wt% at $Na_2O/K_2O \sim 1$. The inclusions from sample N-2 show a monotonous increase in Na/K with increasing degree of melt differentiation (Fig. 6). This suggests that the melt was depleted in K_2O owing to the fractionation of a potassic phase. Samples N-3, N-4, and Gyd-2 display a different trend: K/Na either does not change or decreases with increasing degree of differentiation. This trend is attributed to simultaneous crystallization of nepheline and potassic phases (biotite or orthoclase).

The initial concentration of TiO_2 in the melts is about 4wt%, and the most evolved melts contain up to 5.5wt% TiO_2 (sample N-7).

Table 7 Representative compositions of glasses from homogenized melt inclusions in olivine, wt%

Sample	N-2	N-2	N-3	N-3	N-3	N-4	N-4	N-4	N-6	N-7	N-7	Gyd-2	Gyd-2	Gyd-2
	1	2	3	4	5	6	7	8	9	10	11	12	13	14
SiO_2	39.72	37.74	36.95	38.48	39.38	39.54	38.41	39.09	39.68	39.42	38.84	44.67	44.25	43.34
TiO_2	4.95	4.84	4.39	4.48	4.79	4.13	4.71	4.03	4.60	4.58	4.40	4.35	3.94	3.68
Al_2O_3	14.54	13.99	13.23	13.49	15.12	14.65	14.12	11.90	13.91	14.41	14.39	17.72	16.91	15.58
FeO	11.13	11.74	12.47	9.84	9.85	11.63	13.75	13.44	10.99	8.75	10.81	6.92	5.71	8.52
MnO	0.14	0.11	0.19	0.09	0.12	0.15	0.14	0.22	0.13	0.10	0.20	0.08	0.08	0.13
MgO	7.45	7.16	5.68	10.03	6.14	9.67	5.63	9.68	6.60	7.76	6.23	8.35	8.10	7.77
CaO	12.14	12.44	13.93	11.99	13.37	11.96	12.67	11.30	11.85	13.09	12.54	10.99	12.85	13.00
Na_2O	5.23	6.63	5.49	6.24	6.26	4.43	6.06	4.77	5.25	7.10	5.94	4.58	4.72	4.42
K_2O	3.08	3.50	2.44	2.74	3.56	2.63	3.40	2.72	2.93	2.66	2.45	3.58	2.70	2.70
S	0.25	0.21	n. d.	n. d.	0.15	0.08	0.20	0.09	0.22	0.19	0.24	0.10	0.12	0.17
Cl	0.13	0.12	0.09	0.13	0.13	0.10	0.13	0.12	0.00	0.11	0.13	0.08	0.14	0.13
F	0.26	0.14	0.06	0.18	n. d.	0.08	0.52	0.21	n. d.	0.27	0.39	n. d.	0.23	0.12
P_2O_5	1.61	1.52	0.78	0.80	n. d.	2.50	1.27	3.00	n. d.	1.64	1.61	n. d.	1.73	1.64
Total	100.63	100.13	95.70	98.46	98.88	101.54	101.00	100.56	96.16	100.08	98.17	101.41	101.49	101.20
T℃	1180	1170	1200	1200	1190	1200	1210	1200	1200	1170	1180	1220	1210	1210
mg Ol	0.86	0.85	0.79	0.84	0.79	0.81	0.78	0.77		0.82	0.82	0.80	0.85	0.86
Compositions recalculated to equilibrium with host olivine														
SiO_2	39.20	37.54	38.42	38.94	39.86	38.88	37.74	38.94	—	39.38	39.40	44.84	44.01	42.78
TiO_2	4.49	4.50	4.41	5.17	5.16	4.59	4.45	4.69	—	5.10	4.40	5.04	4.41	3.69
Al_2O_3	13.19	13.02	13.30	15.55	16.29	16.26	13.33	13.87	—	16.03	14.39	20.55	18.90	15.66
FeO	11.92	12.38	13.54	8.57	8.85	9.86	14.19	11.08	—	7.26	11.19	4.35	4.01	8.16
MnO	0.13	0.11	0.20	0.09	0.12	0.15	0.13	0.22	—	0.11	0.20	0.08	0.08	0.13
MgO	9.93	9.05	6.84	5.86	4.21	5.79	6.59	5.06	—	4.06	6.76	2.43	3.12	7.00
CaO	11.03	11.59	14.02	13.79	14.38	13.25	11.98	13.12	—	14.54	12.55	12.71	14.33	13.07
Na_2O	4.74	6.17	5.52	7.20	6.75	4.92	5.72	5.56	—	7.91	5.94	5.32	5.28	4.45
K_2O	2.79	3.25	2.46	3.17	3.83	2.93	3.21	3.18	—	2.97	2.45	4.16	3.02	2.72
S	0.27	0.22	0.00	0.00	0.14	0.07	0.20	0.08	—	0.17	0.25	0.08	0.11	0.16
Cl	0.11	0.11	0.09	0.15	0.14	0.11	0.12	0.14	—	0.12	0.13	0.09	0.16	0.13
F	0.24	0.13	0.06	0.21	–	0.09	0.49	0.25	—	0.30	0.39	—	0.26	0.12
P_2O_5	1.46	1.52	0.78	0.92	–	2.77	1.20	3.50	—	1.83	1.61	—	1.93	1.65

Table 8 Concentrations of trace elements in the glasses of homogenized melt inclusions in olivine, ppm

Sample	N-2	N-2	N-4	N-4	N-4	N-3	N-7	Gyd-2	Gyd-2
	1	2	3	4	5	6	7	8	9
La	75.50	55.40	75.16	77.73	73.58	70.07	88.48	39.84	34.55
Ce	151.02	110.65	143.87	181.77	143.50	146.56	188.80	76.95	69.04
Nd	74.69	55.72	73.54	75.71	74.84	68.40	88.87	35.31	30.95
Sm	14.70	12.10	13.71	18.28	14.19	17.09	21.19	8.02	6.70
Eu	4.80	3.06	4.21	4.53	5.24	4.66	5.76	2.64	2.05
Gd	13.60	8.47	11.65	17.09	10.05	15.00	16.56	7.73	6.27
Dy	8.85	6.09	7.26	8.09	7.80	8.17	10.46	4.91	4.37
Er	3.73	2.61	2.16	4.55	2.99	3.36	4.88	1.92	2.11
Yb	2.30	1.72	1.38	1.05	1.81	1.50	2.34	3.00	1.40
Cr	815.8	1147.3	519.5	1892.6	415.3	1404.0	273.1	535.6	803.7
Rb	51.06	70.26	59.02	124.63	44.67	79.30	46.48	47.26	42.94
Sr	1589.4	1184.0	1611.5	1985.6	1552.8	1605.3	1969.4	890.7	724.7
Zr	385.5	277.9	371.8	451.2	372.0	381.8	451.4	178.7	148.2
Ba	692.3	552.5	743.1	898.0	627.3	741.3	881.3	610.6	543.3
Th	5.94	4.21	5.44	6.64	5.08	5.70	7.73	3.19	3.25
U	1.95	1.62	2.31	1.77	2.21	2.25	2.67	1.47	1.45
Ta	4.11	3.43	4.36	4.63	4.11	4.19	5.14	2.52	2.30
Hf	7.50	5.07	6.80	8.26	8.09	6.61	9.06	3.71	3.38
Nb	114.66	90.27	125.59	126.03	120.35	108.51	139.44	70.18	62.65
Y	36.78	26.18	27.50	36.95	33.85	30.61	42.19	22.01	18.20
B	4.07	13.12	3.42	3.54	2.71	9.11	9.00	3.91	18.51
V	300.84	176.10	251.40	235.20	146.25	203.41	305.92	213.17	210.75
H_2O, wt%	0.03	0.01	0.03	0.16	0.03	0.04	0.14	0.22	0.13
F, wt%	0.18	0.11	0.14	0.10	0.10	0.09	0.19	0.19	0.13

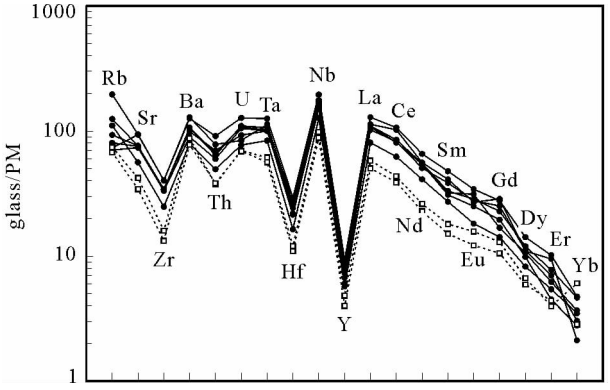

Fig. 7 Primitive mantle normalized patterns of trace elements in the glasses of heated melt inclusions in olivine. The dashed lines show concentrations in sample Gyd-2.

The concentrations of trace elements in the glasses of inclusions are given in Table 8. Fig. 7 shows their primitive mantle normalized distribution patterns. All the melts are enriched in REE (REE total is up to 430 ppm), especially in LREE (La_N/Yb_N up to 73). The melts have high Ba, Nb, Rb, U, Ta, and Sr and low Zr, Hf, and Y concentrations.

5 Discussion and Conclusions

All the melts trapped in phenocrysts show a number of common features. They are strongly silica-undersaturated and rich in alkalis, titanium, and some other minor elements. A common peculiarity of all the samples is the overabundance of CO_2, which occurs as bubbles in groundmass and numerous primary and secondary inclusions in phenocrysts. In general, these features are typical of intraplate magmas related to mantle plume activity.

5.1 Compositions of primary melts

The compositions of primary melts can be constrained by assuming the equilibrium with source minerals. If the primary melanephelinite magmas were derived by low-degree melting of the continental lithospheric mantle, the residual olivine probably had an mg value of about 0.91 (Gaul *et al.*, 2000). Then, the composition of the deep-derived primary melt can be estimated by adding olivine to the most primitive melts trapped in olivine to reach the equilibrium $K_D = (Fe/Mg)^{Ol}:(Fe/Mg)^{Liq}$ value. Table 9 shows the calculated average compositions of primary melts for each sample.

There are some differences between the calculated primary melts. Three samples (N-2, N-3, and N-4) are similar to each other in major and trace-element characteristics. They show lower concentrations of SiO_2, Al_2O_3, TiO_2, CaO, K_2O and higher concentrations of MgO, FeO, and Cl compared with sample Gyd-2 (Fig. 8a). Correspondingly, sample Gyd-2 has the highest SiO_2 and lowest MgO and FeO concentrations. Sample N-7 is transitional in terms of many major-element characteristics, but it has relatively high TiO_2, Na_2O, F, and incompatible trace element contents (Fig. 8b).

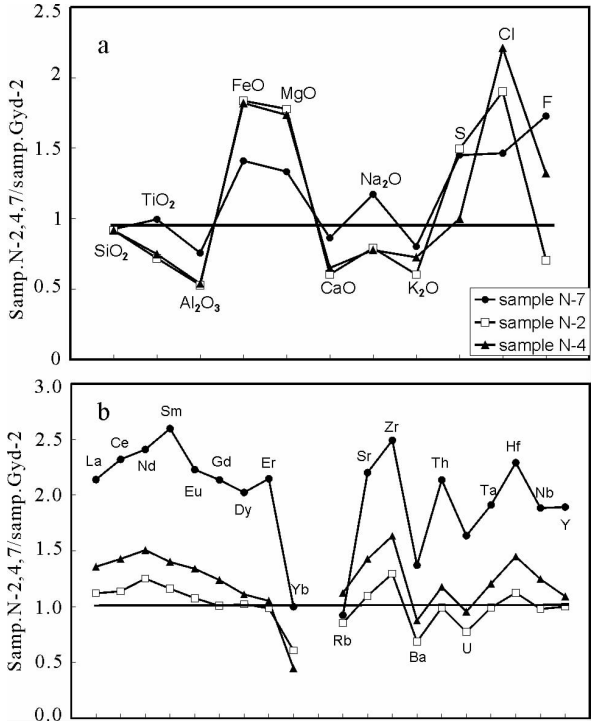

Fig. 8 Concentrations of (a) major and (b) trace elements in the calculated primary melts for samples N-2, N-4, and N-7 normalized to the composition of the primary melt for sample Gyd-2.

Despite some differences, the compositions of all the primary melts are similar (Fig. 7), which suggests their derivation from a common source.

Table 9 Compositions of primary melts, wt%

	N-7	N-2	Gyd-2
SiO_2	39.42	39.32	41.79
TiO_2	1.75	2.72	2.59
Al_2O_3	5.72	8.01	10.99
FeO	16.12	13.94	10.89
MnO	0.20	0.12	0.12
MgO	27.52	22.73	17.62
CaO	4.72	6.77	9.23
Na_2O	2.14	2.87	3.11
K_2O	0.95	1.69	1.90
P_2O_5	0.66	0.89	1.16
S	0.52	0.42	0.23
BaO	0.10	0.12	0.08
F	0.08	0.14	0.08
Cl	0.04	0.07	0.09
SrO	0.06	0.20	0.11
Total	100.00	100.00	100.00

Note: The compositions were calculated from the analyses of the least evolved melts trapped in olivines from respective samples by adding olivine up to the equilibrium with mantle olivine, Fo90 at 35 kbar.

5.2 Volatile components in magmas

A number of observations suggest that the magmas were saturated with fluid and experienced extensive degassing during a significant portion of their magmatic history. Among such observations are the abundance of primary high-density CO_2 inclusions in olivine, low-density fluid inclusions along healed fractures in olivine, and numerous vesicles in the rock groundmass. Similar features were described by Solovova *et al.* (2003) in the olivine melilitite of Mahlberg, Germany. The samples discussed here bear some resemblance to popping rocks recovered from the ocean floor (Pineau *et al.*, 1976; Javoy *et al.*, 1991; Dixon *et al.*, 1997; Moreira *et al.*, 1998). These are alkali basaltoids and nephelinites containing numerous vesicles filled with high-density CO_2. Dixon *et al.* (1997) estimated the initial contents of CO_2 and H_2O in the primary melts of the North Arch volcanic field, Hawaii as 5.4 and 1.9wt%, respectively. This CO_2 content is practically identical to a value of 5.5wt% obtained by Kovalenko *et al.* (1987) for mantle melts on the basis of melt inclusions in mantle xenoliths.

The highest density of CO_2 in the partly decrepitated primary fluid inclusions ($0.93 g/cm^3$) corresponds to a pressure of 800MPa at a temperature of 1230℃. Using Papale's (1997) model, the CO_2 content of the olivine melanephelinite melt can be estimated as up to 2.5wt% at these conditions. The abundance of fluid inclusions suggests that the magma could be heterogeneous before the beginning of olivine crystallization. In such a case, the initial CO_2 content of 2.5wt% is the minimum constraint. Using Brey and Green's (1975) solubility model, the CO_2 content is estimated as more than 5wt%.

The measured H_2O contents in the glasses of inclusions are very low (Table 8). There is some evidence that H_2O can escape from melt inclusions during magma crystallization and thermometric experiments (Massare *et al.*, 2002). The durations of out experiments were always below 15 min to minimize hydrogen loss. The absence of hydrous phases (amphibole or phlogopite) in the lavas (Akinin, 1994) is also indicative of low H_2O content in the initial olivine melanephelinite magma. Thus, we conclude that the magmas were rich in CO_2 (>2.5wt%) and relatively water-poor.

5.3 Mantle source

Akinin (1994), Akinin *et al.* (1997), and Apt *et al.* (1998) studied mantle xenoliths from the alkaline volcanics of the Chukchi Peninsula. The xenolith suite includes spinel-facies lherzolites and garnet pyroxenites. The high LREE/HREE ratios of the inclusion glasses suggest that the melts were derived from a garnet-bearing source material. Therefore, the spinel lherzolites were probably entrained by the magma en route to the surface and could be different from the magma source. Both garnet lherzolite and pyroxenite can produce alkaline magmas with low silica content (Walter, 1998; Keshav *et al.*, 2004). The available data do not allow us to determine unambiguously the lithology of the mantle source. Moreover, the difference between the compositions of primary melts of Gyd-2 and other samples could be related to different source compositions (pyroxenitic and lherzolitic, respectively). Alternatively, they could be derived from a common source under different conditions (SiO_2-poor melts from a deeper and hotter zone of the mantle plume and SiO_2-rich melts from a colder zone).

The relatively high concentrations of strongly incompatible trace elements with high Ce/Y and low Zr/Nb ratios can be produced by very low degrees of melting (~1%) of a primitive or slightly depleted source (Hardarson and Fitton, 1991). However, some compositional parameters seem to be at odds with a primitive or depleted mantle source. The most conspicuous among them is the low ratio of H_2O to other highly incompatible elements (e.g., H_2O/Ce) and high concentration of CO_2. It is therefore necessary to suppose a preliminary enrichment of the magma source in CO_2 and other incompatible elements. The concept of mantle metasomatism is often invoked to explain the enriched characteristics of alkaline magmas. Some geochemical indicators can be used to discriminate between water-rich and CO_2-rich metasomatizing fluids. In addition to the high CO_2 content and CO_2/H_2O ratio, high Sr and Nb and low Zr concentrations favour the CO_2-rich composition of metasomatizing fluid (Downes *et al.*, 2002) (Fig. 9).

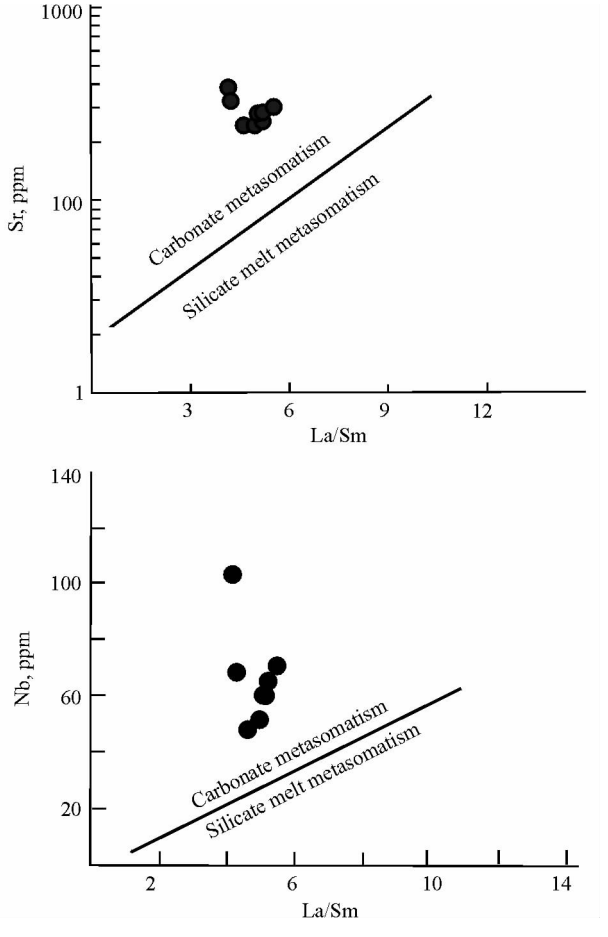

Fig. 9 Concentrations of Sr and Nb as functions of La/Sm ratios for the primary melts of the olivine melanephelinites. The fields of mantle sources metasomatized by carbonate and silicate melts are after Downes *et al.* (2002).

5.4 Conditions of melt generation

Although the composition of the mantle source is poorly

constrained, melting conditions can be estimated assuming that the source material is not very different from a primitive or slightly depleted mantle peridotite. A comparison with Walter's (1998) experimental data shows that liquids similar to the primary melts of samples N-2, N-4, and N-6 can be produced by low-degree melting (1 ~ 5%) of garnet-bearing lherzolite at 1480 ~ 1520℃ and 3.5 ~ 4.0GPa. The composition of melt from sample Gyd-2 can be derived at 2.5 ~ 3.0GPa and 1440℃.

Acknowledgement We thank E. Libowitzki (Institute of Mineralogy, University of Vienna, Austria) for recording the Raman spectrum of one fluid inclusion. This study was financially supported by the Russian Foundation for Basic Research and Russian Program for the Support of Leading Scientific Schools.

References

Akinin VV. 1994. Petrology of alkali lavas and deep-seated inclusions of Enmelen volcanoes, Chukchi Peninsula. In: Proceedings of ICAM 94. Late Cenozoic Basic & Ultrabasic Volcanism, 138 – 146

Akinin VV, Apt JE. 1994. Enmelen volcanoes, Chukchi Peninsula: Petrology of alkaline lavas and deep-seated inclusions. NEISRI FEB RAS, Magadan, 97 p

Akinin VV, Roden MF, Francis D, Apt J, Moll-Stalcup E. 1997. Compositional and thermal state of the upper mantle beneath the Bering Sea basalt province: evidence from the Chukchi Peninsula of Russia. Can. J. Earth Sci., 34: 789 – 800

Apt Yu E, Akinin VV, Wright JE. 1998. Sr, Nd and Pb isotopes in Neogene melanephelinites and deep-seated xenoliths from northeast Russia. Geochemistry International, 36(1): 24 – 33

Brey GP, Green DH. 1975. The role of CO_2 in the genesis of olivine melilitite. Contrib. Mineral. Petrol., 49: 93 – 103

Dixon JE, Clague DA, Wallace P, Poreda R. 1997. Volatiles in alkalic basalts from the North Arch volcanic field, Hawaii: extensive degassing of deep submarine-erupted alkalic series lavas. J. Petrol., 38: 911 – 939

Downes H, Kostoula T, Jones A, Bread AD, Thirlwall MF, Bodinier J-L. 2002. Geochemistry and Sr-Nd isotopic compositions of mantle xenoliths from the Monte Vulture carbonatite-melilitite volcano, central southern Italy. Contrib. Mineral. Petrol., 144: 78 – 92

Fedorov PI, Koloskov AV, Lyapunov SM. 1993. Geochemistry and petrology of the Late Cenozoic volcanics of the Navarin Cape (eastern Karyak Highland). Geokhimiya, (9): 1284 – 1297

Fedorov PI, Seregina IF. 1990. Geochemistry of the Late Cenozoic volcanics of the Navarin Cape (Karyak Highland). Geol. Geofiz., 3: 94 – 100

Feeley TC, Winer GS. 1999. Evidence for fractionation of Quaternary basalts on St. Paul Island, Alaska, with implications for the development of shallow magma chambers beneath Bering Sea volcanoes. Lithos, 46: 661 – 676

Gaul OF, Griffin WL, O'Reilly SY, Pearson NJ. 2000. Mapping olivine composition in the lithospheric mantle. Earth Planet. Sci. Lett., 182: 223 – 235

Hardarson BS, Fitton JG. 1991. Increased mantle melting beneath Snaefellsjokull volcano during Late Pleistocene glaciation. Nature, 353: 62 – 64

Javoy M, Pineau F. 1991. The volatile record of the popping rock from the Mid-Atlantic Ridge at 14N: chemical and isotopic compositions of gasses trapped in the vesicles. Earth Planet. Sci. Lett., 107: 598 – 611

Kay RW, Sun S-S, Lee-Hu C-N. 1978. Pb and Sr isotopes in volcanic rocks from the Aleutian Islands and Pribilof Islands, Alaska. Geochim. Cosmochim. Acta, 42: 263 – 273

Keshav S, Gudfinnsson G, Sen G, Fei Y. 2004. High-pressure melting experiments on garnet clinopyroxenite and the alkalic to tholeiitic transition in ocean-island basalts. Earth Planet. Sci. Lett., 223: 365 – 379

Kovalenko VI, Solovova IP, Naumov VB, Ryabchikov ID, Ionov DA, Bogatikov OA. 1987. Fluidized CO_2-sulfide-silicate media as a course of mantle metasomatism and formation of megacrysts evidence from a composite xenolith and megacrysts from Central Mongolia. Phys. Earth Planet. Int., 45: 280 – 293

Massare D, Metrich N, Clocchiatti R. 2002. High-temperature experiments on silicate melt inclusions in olivine at 1 atm: inference on temperatuter of homogenization and H_2O concentrations. Chem. Geol., 183: 87 – 98

Melnik Yu P. 1978. Thermodynamic properties of gases under conditions of deep petrogenesis. Naukova Dumka. Kiev. 150 p

Moll-Stalcup EJ. 1994. The origin of the Bering Sea basalt province, western Alaska. In: Simakov KV, Thurston DK (Eds.). Proc. Int. Conf. Arc. Mar., 113 – 123

Moreira M, Kunz J, Allegre C. 1998. Rare gas systematics in popping rock: isotopic and elemental compositions in the upper mantle. Science, 279: 1178 – 1181

Papale P. 1997. Modeling of the solubility of a one-component H_2O or CO_2 fluid in silicate liquids. Contrib. Miner. Petrol., 126: 237 – 251

Pineau F, Javoy M, Bottinga Y. 1976. $^{13}C/^{12}C$ ratios of rocks and inclusions in popping rocks of the Mid-Atlantic Ridge and their bearing on the problem of deep-seated carbon. Earth Planet. Sci. Lett., 29: 413 – 421

Shmonov V M, Shmulovich K I. 1974. Molar volumes and equation of state of CO_2 at temperatures from 100 ~ 1000℃ and pressures from 2000 ~ 10,000 bars. Dokl. Akad. Nauk, 217: 206 – 209

Solovova IP, Girnis AV, Rass IT, Keller J, Kononkova NN. 2003. Different styles of evolution of CO_2-rich alkaline magmas: the role of melt composition in carbonate-silicate liquid immiscibility. Periodico di Mineralogia, 72: 87 – 93

Walter MJ. 1998. Melting of garnet peridotite and the origin of komatiite and depleted lithosphere. J. Petrol., 39: 29 – 60